Hindawi
Advances in Materials Science and Engineering
Volume 2018, Article ID 8467921, 9 pages
https://doi.org/10.1155/2018/8467921

Research Article

Friction Characteristics of Synchronization Process Based on Tribo-Thermodynamics

Hao Yan,[1] Zhaoping Xu,[1] Juntang Yuan,[1] Liang Liu,[1] Cao Tan,[2] and Wenqing Ge[2]

[1]*School of Mechanical Engineering, Nanjing University of Science and Technology, Nanjing 210094, China*
[2]*School of Transportation and Vehicle Engineering, Shandong University of Technology, Zibo 255000, China*

Correspondence should be addressed to Zhaoping Xu; xuzhaoping@njust.edu.cn

Received 11 April 2018; Revised 26 June 2018; Accepted 4 July 2018; Published 7 August 2018

Academic Editor: David Holec

In order to improve the shift control accuracy and shift quality, the temperature and friction coefficient changing regularities of a friction cone during the synchronization process were investigated. The thermal-structural coupling model was established through tribo-thermodynamic analysis. The relevant experiment was carried out as well. The results show that the error between the experimental and simulated results is within 3%. Besides, the maximum temperature of the synchronous ring friction surface increases 1.8°C for every additional 50 N of shift force, while increases 1.1°C for every additional 200 r/min shift speed difference. Moreover, the friction coefficient declines rapidly first and then tends to be stable slowly during the synchronization process. The result of friction coefficient changing regularity lays a good theoretical basis for establishing an effective friction coefficient compensation control strategy.

1. Introduction

Transmission is an important part of the transmission system and has been regarded as the focus of technological innovation for a long time [1, 2]. The shift speed difference is eliminated by the interaction of a synchronizer friction cone during the synchronous shift phase. The heat generated by friction will change material surface energy and lattice resistance, so that the friction coefficient between friction cones will change and the shift control accuracy of transmission will be influenced [3].

Currently, lots of researches to improve the automatic transmission's control accuracy have been proposed [1–3]. The friction surface temperature and the friction coefficient of the friction cone are the critical influences on the shift control accuracy and shift quality. In the literature [4–6], the temperature changing regularities of the friction surface under different working conditions were analyzed by simulation and experiment. The influence of temperature on synchronizer working performance was verified. In the literature [7, 8], the friction and heat generation process of the synchronizer with different friction coefficients were analyzed by simulation. The results show that the greater the friction coefficient is, within a certain range, the higher the temperature between the friction surfaces is. The friction characteristics of the synchronizer were preliminary studied in the above literatures. However, the influence of friction heat and friction coefficient on the accuracy of synchronous shift control was rarely considered during the synchronization process.

The friction coefficient of the synchronizer friction cone is an important index in the synchronizer. Li et al. present a model of predicting wear in the friction lining of a wet clutch and introduces that the wear mechanism is related to thermal degradation [9, 10]. Marklund and Larsson develop a friction model which takes temperature, speed, and nominal pressure into account of the wet clutch during boundary lubrication conditions [11, 12]. The investigation of temperature and friction coefficient during the synchronization process will lay a good theoretical basis for establishing a control strategy for automotive transmission designers.

This paper is organized as follows. Section 2 describes the existing problem of the locking ring synchronizer.

The thermal-structural coupling model is established through tribo-thermodynamic analysis in Section 3. The established model is verified by experiments in Section 4. The analysis of results is carried out in Section 5. This paper is concluded in Section 6.

2. Problem Description

2.1. Structure and Operating Principle. The locking ring synchronizer of automated mechanical transmission is the research object in this paper. The schematic diagram of the locking ring synchronizer is shown in Figure 1, which consists of a synchromesh sliding sleeve, a splined hub, a synchronous ring, a target ring gear, and a locating slider. The material parameters are shown in Table 1.

During the synchronization process, the synchronous ring is under an axial shift force. The speed difference between the synchronous output shaft and the input shaft is eliminated by the friction torque between synchronous ring's inner cone and target ring gear's friction cone to achieve a smooth and fast shift. Thus, the friction surface temperature and the friction coefficient of the friction cone are the critical influences on the shift control accuracy and shift quality.

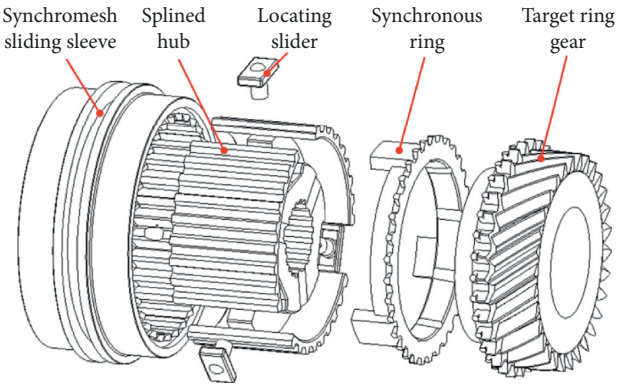

Figure 1: The structure of lock ring synchronizer.

Table 1: Primary material parameters.

Parameters (room temperature)	45 Steel	QSn4-3
Density ρ (kg·m^{-3})	7890	8800
Elastic modulus E (GPa)	209	1100
Poisson ratio (μ_o)	0.27	0.33
Thermal conductivity λ (W·m^{-2}·K^{-1})	48.15	47
Specific heat capacity c (J·kg^{-1}·K^{-1})	450	380
Thermal expansion coefficient (1°C^{-1})	1.08e−5	1.8e−5

2.2. Heat Resource Analysis. In the actual synchronization process, the synchronous force is only the catalyst for energy transfer and transformation of the transmission system. All the work done by the friction torque is converted into irreversible heat loss, which is the primary heat source of the synchronizer [13]. Divide synchronizer friction pair surfaces into microelements, and denote one of them as dA. The normal pressure between synchronizer friction pair surfaces is p, and then the friction dF on the area dA is

$$dF = \mu p\, dA, \tag{1}$$

where μ is the friction coefficient between friction surfaces. Under the influence of friction dF, the moving distance within dt is

$$ds = \omega(t) r\, dt, \tag{2}$$

where r is the average radius of the friction cone. Assuming that all the work done by friction dF converts to heat [14], the heat produced in dt is

$$dQ = dF\, ds = \mu pr\omega(t) dA\, dt. \tag{3}$$

The heat flux function on synchronizer friction pair surfaces is

$$q(r,t) = \frac{dQ}{(dA\, dt)} = \mu pr\omega(t). \tag{4}$$

According to the operating parameters, the heat flux input function of the synchronizer friction pair is determined to be $(3200000 - 6400000 \times t)$ W/m^2·s. Meanwhile, ignoring the heat is taken away by oil in the synchronizer ring thread groove, the heat generated by the metal friction pair is completely absorbed by the synchronizer ring and target gear ring. So that the heat is all assigned to the synchronizer ring and the target ring gear conical surface. The distribution of the heat flux between the synchronizer ring and the conical surface is related to their material properties directly. According to the relevant conclusions [15, 16], the heat flux distribution ratio between upper and lower specimens is

$$k = \frac{q_p}{q_d} = \sqrt{\frac{\lambda_p c_p \rho_p}{\lambda_d c_d \rho_d}}, \tag{5}$$

where subscripts p and d stand for the material properties of the synchronizer ring and target gear ring, λ is the thermal conductivity, c is the specific heat capacity, and ρ is the density. According to Table 1, by substituting (5), the heat flux distribution coefficient of the synchronizer ring is 51%, which of the target gear ring is 49%.

3. Thermal-Structural Coupling Model

3.1. Heat Transfer Modeling. In Cartesian coordinates, take any microelement on the surface of the friction pair as the research object. According to the law of conservation of energy, the heat balance relationship of microelements in unit time is analyzed [17, 19]. Select first gear for second gear as the typical working condition of thermal-structural coupling analysis of the synchronizer, and calculate the boundary conditions in the synchronization process. The temperature of friction pair surfaces changes with time. As for the transient heat conduction problem [13], to solve the problem of temperature field distribution without internal heat source, the heat conduction equation is

$$\frac{\rho c}{\lambda}\frac{\partial T}{\partial t} = \frac{\partial^2 T}{\partial x^2} + \frac{\partial^2 T}{\partial y^2} + \frac{\partial^2 T}{\partial z^2}, \quad (6)$$

where T is the thermodynamic temperature. The thermal conduction differential equation is a general expression to describe the conduction process but does not involve a specific conduction process. For solving the specific thermal conduction differential equation, declaration conditions are needed to obtain a unique solution.

The heat flux is affected by parameters such as speed, pressure, and friction coefficient, and it is time dependent. It is an unsteady heat conduction process, which accords with the second boundary condition. For convection heat transfer boundary conditions, the convective heat transfer coefficient equation and the operational environment temperature are known, and the real-time convective heat transfer coefficient at the synchronizer boundary can be obtained, which belonged to the third boundary condition.

The convective heat transfer coefficient mainly depends on fluid states, the physical properties of fluid, the geometrical factors of the heat transfer surface, the cause of flow, and whether the fluid has a phase change [17]. The convective heat transfer coefficient is calculated as follows:

$$h_{\text{con}} = \frac{\text{Nu}\lambda_{\text{air}}}{l}, \quad (7)$$

where Nu is the Nusselt number, λ_{air} is the air thermal conductivity, and l is the characteristic length of the heat transfer surface. Convective heat transfer is divided into three categories: (1) forced convection heat transfer; (2) natural convection heat transfer; and (3) mixed convection heat transfer. The convection heat transfer manner is usually determined by the value of Gr/Re^2 in engineering [18]. The Grashof number Gr is calculated as follows:

$$\text{Gr} = \frac{g\alpha_v \Delta t l^3}{\eta_{\text{air}}^2}, \quad (8)$$

where g is the acceleration of gravity, Δt is the temperature difference between thermal conductivity object and the environment, and η_{air} is the kinematic viscosity of air in normal temperature. When v is the velocity, the Reynolds number Re is calculated as follows:

$$\text{Re} = \frac{vl}{\eta_{\text{air}}}. \quad (9)$$

In order to simplify the calculation of thermo-structural coupling analysis of the synchronization process, the target ring gear is assumed to be stationary and the synchronizer ring is rotating. The speed of the synchronizer ring is equal to the speed difference between the two ends of the synchronizer during the actual synchronization process. Hence, there is no relative motion between the target ring gear and the surrounding air. There is a natural convection heat transfer between the target ring gear surface and the air [19]. The surface shape of the target ring gear friction cone is cylindrical vertical wall, and air flow is laminar. The Nusselt number for natural convection heat transfer is calculated as follows:

$$\text{Nu} = 0.68 + \frac{0.67\,(\text{Ra})^{1/4}}{[1 + (0.492/\text{Pr})]^{4/9}}, \quad (10)$$

where Pr is the Prandtl number and Ra is the Rayleigh number. Ra is calculated as

$$\text{Ra} = \text{Gr} \cdot \text{Pr}. \quad (11)$$

When the synchronous ring speed is 200 r/min, the Reynolds number is 186.67, the Grashof number is 1563, and Gr/Re^2 is 0.045. There is a forced convection heat transfer between the synchronizer ring surface and the air because Gr/Re^2 is less than 0.1 [19]. Besides, the speed between the two ends of the synchronizer is more than 200 r/min during the synchronization process. Substituting the results of the Grashof number calculated into (11), the Rayleigh number 11095.8 can be obtained. Nusselt number 6.08 can be obtained by substituting the Rayleigh number into (10). Finally, the free convection heat transfer coefficient (h_{con}) of the target gear ring is 6.08 $\text{W/m}^2\cdot\text{K}$.

C is the coefficient of the constant term. The Nusselt number of forced convection heat transfer is calculated as follows:

$$\text{Nu} = C\text{Re}^{1/2}\text{Pr}^{1/3}. \quad (12)$$

Similarly, the forced convection heat transfer coefficient (h_{con}) of the synchronizer ring is 28.96 $\text{W/m}^2\cdot\text{K}$.

3.2. 3D Finite Element Model. The thermo-structural coupling modeling based on 3D finite element method is carried out through the above theoretical analysis. Firstly, a three-dimensional model of the synchronizer is established based on CATIA. Then, the target ring gear is 45 Steel as material, and the synchronous ring is copper alloy (QSn4-3) [20]. Their primary material parameters are shown in Table 1.

Moreover, the mesh model of the target ring gear and synchronous ring is shown in Figure 2, as well as the boundary conditions. Besides, the selection of the boundary condition has been explained in Section 3.1. The boundaries 1 and 6 are friction interfaces. The heat resource is applied to friction interfaces. The boundary 2–5 of the synchronous ring is the forced convection heat transfer boundary, while the boundary 7–9 of the target ring gear is the natural convection heat transfer boundary.

4. Experimental Verification

4.1. Experimental Setup. In order to verify the accuracy of the thermal-structural coupling model and investigate friction coefficient change regularities of the friction cone, the synchronization process is researched by the friction and wear test bench. The schematic of the experimental setup is shown in Figure 3.

The experimental setup of the synchronizer mainly consists of a three-phase asynchronous motor (Y90L-4) that simulates input shaft speed, an inertia simulator at input shaft (the range of rotational inertia 0.04~0.09 $\text{kg}\cdot\text{m}^2$), a gear shift simulator, a linear actuator (AUM5-S2) that simulates

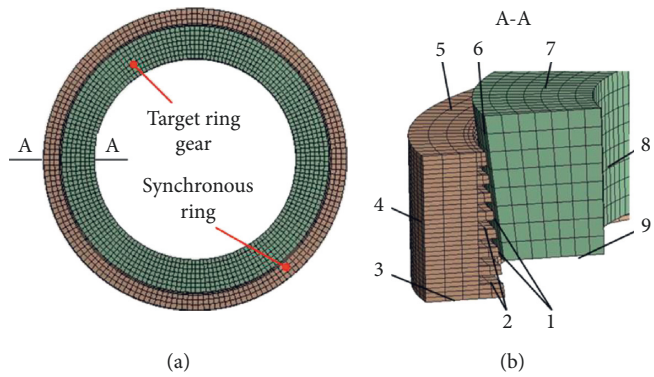

Figure 2: The mesh generation and boundary conditions of the synchronizer. 1, 6: heat resource (friction interfaces); 2–5: forced convection heat transfer boundary; 7–9: natural convection heat transfer boundary.

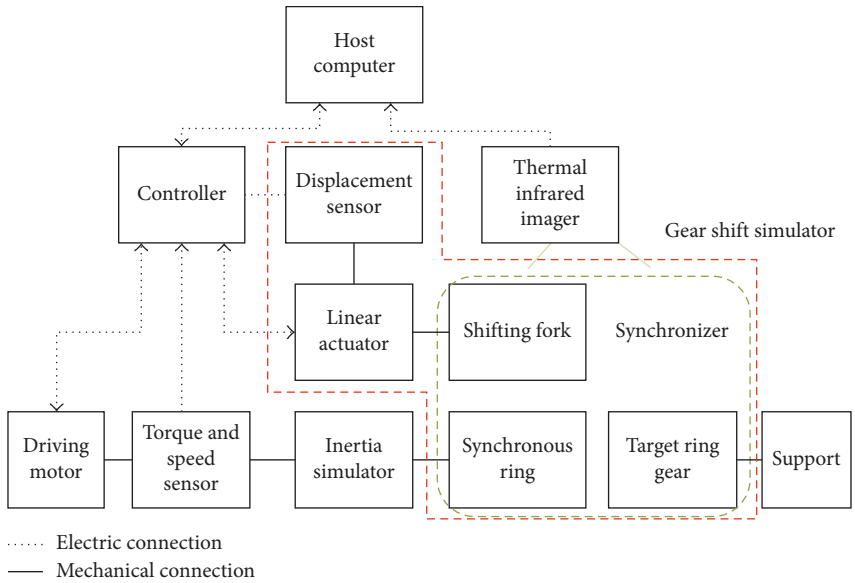

Figure 3: Schematic of experimental setup.

shift force, and a support for target ring gear. To verify the model, following signals are acquired from the experiment setup: a thermal infrared imager (Optris PI 450), a displacement sensor (WYDC-15D), and a torque-speed sensor (JN338-300A) with a 0.1% FS and 300 N·m (5000 *r*/min) measuring range. Besides, a controller and a host computer are needed to control the experimental process and collect data. Set the required inertia value and speed difference before test. Open the three-phase asynchronous motor to drive input shaft by the controller. When the feedback signal from the torque-speed transducer reaches to predetermined speed value, turn off the three-phase asynchronous motor and turn on the linear actuator. The required shift force is provided through the linear actuator. The host computer receives the feedback signal from each sensor to realize real-time control during the synchronization process. The photo of the experimental setup is shown in Figure 4.

The test bench adopts a ring-ring friction pair structure, and the size of the test specimen is basically the same as the size of the car synchronizer. According to the actual synchronization process, adjust the speed and the shift force, so that the test operation is closer to the real synchronization process. The tests were carried out at room temperature. There must be no strong light around specimens; otherwise, reflection may cause inaccurate measurements. The relevant parameters of the synchronizer ring and the target gear ring are shown in Table 2.

4.2. Model Verification. Take the condition that the synchronous load is 195 N and the speed difference is 1000 *r*/min as an example. The temperature distribution of the synchronizer measured by the infrared thermal imager at a certain time is shown in Figure 5.

The temperature measuring areas 1 and 2 ($1 \times 1\,\text{mm}^2$) measure the change of maximum temperature on the frictional cone during the synchronization process. Temperature measuring area 3 measures the change of average temperature on the target gear ring liner cone. In the right corner of Figure 6, 21.67°C represents the average temperature in the temperature measuring area 3. In order to verify the accuracy of the simulation results, the experimental and

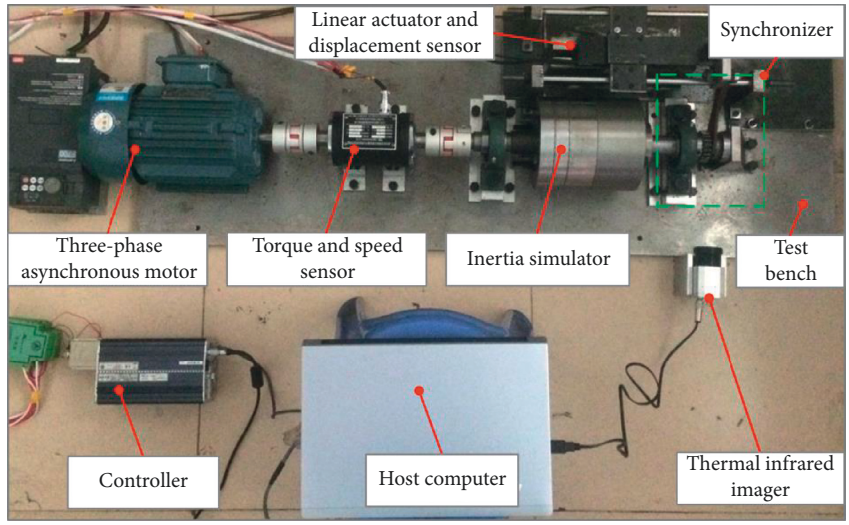

Figure 4: Schematic of experimental setup.

Table 2: Specification parameters.

Parameters	Synchronizer ring	Target gear ring
Material	QSn4-3	45 Steel
Inner diameter (external diameter) (mm)	13	26
Min external diameter (min inner diameter) (mm)	20	20
Max external diameter (max inner diameter) (mm)	21	21
Axial length (mm)	8	28

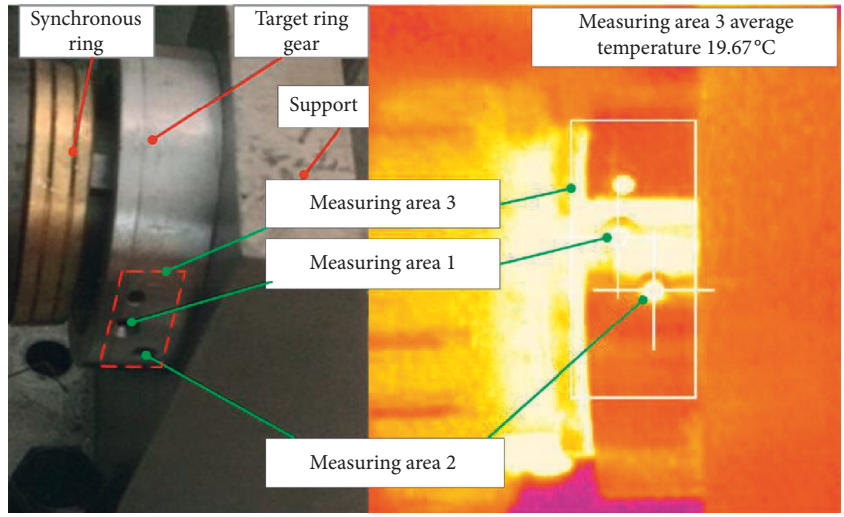

Figure 5: The thermal imagery taken by thermal imager.

simulated results of maximum temperature on the frictional cone during the synchronization process are shown in Figure 7.

There are errors between the experimental and simulated results of the friction cone temperature field during the synchronization process. The error between the experimental and simulated results is controlled within 3%, which verifies the accuracy of thermo-structural coupling analysis. There are two main reasons that lead to the error. Firstly, the wear-resistant treatment is not applied to the friction cone of synchronous ring and target gear ring in the experimental study. There are microbulges on the friction cone, so that the actual friction contact area is less than the ideal contact area. Secondly, the forced convection heat transfer coefficient of the synchronous ring friction cone is related to speed, according to formulas (9) and (13). The slower the rotational speed is, the smaller the convection heat transfer coefficient is. However, the convective heat transfer coefficient of the synchronous ring surface is set to a constant value in simulation, while the convective heat transfer coefficient of

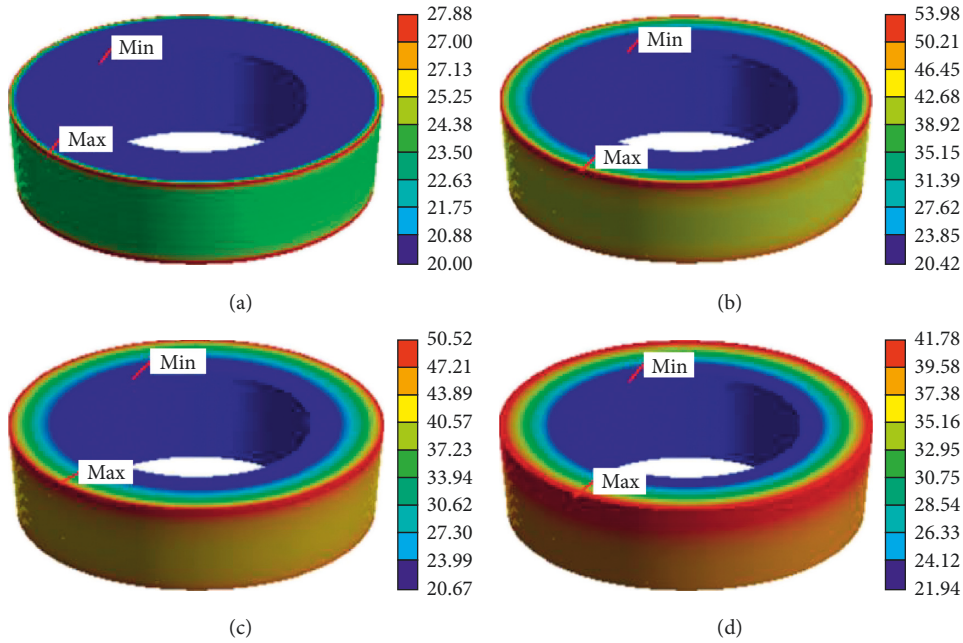

Figure 6: Surface temperature distribution of the target gear ring. (a) $t = 0.035$ s, (b) $t = 0.678$ s, (c) $t = 1.143$ s, and (d) $t = 1.5$ s.

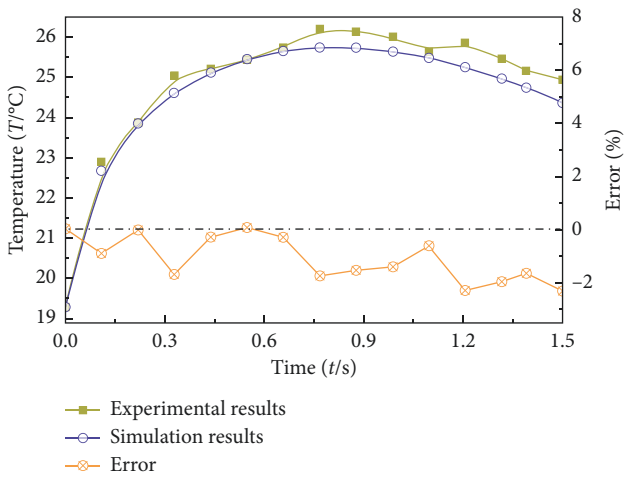

Figure 7: Comparison of experimental and simulated results.

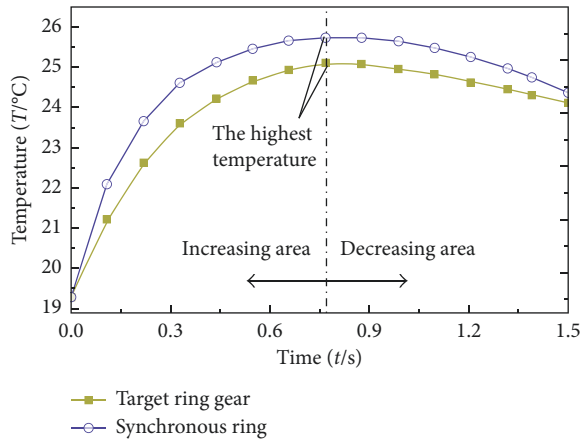

Figure 8: The highest temperature changing regularities of friction surface.

the synchronous ring surface is changing all the time during the practical tests.

5. Results and Discussion

5.1. Temperature Rise Analysis. Take the condition that the synchronous load is 195 N and the speed difference is 1000 r/min as an example. The highest temperature changing regularities of friction surface through the thermo-structural coupling analysis is shown in Figure 8. The temperature of the target gear ring and synchronous ring at different time is shown in Figures 6 and 9, respectively.

The maximum temperature changing regularities of the synchronizer ring and target gear ring are the same. The temperature increases first and then decreases. At the initial stage of friction, the energy of heat flux density input is greater than the energy of heat conduction and convective heat transfer taken away, and the temperature increases speedily. With the decrease of speed difference at both ends of the synchronizer, heat flux and convective heat transfer coefficient of the friction cone decreases gradually. When the energy of heat flux density input is equal to the energy taken away, the temperature of the synchronizer ring friction cone reaches to the maximum. As the speed difference at both ends of the synchronizer decreases continuously, the temperature of the synchronizer ring friction surface reduces gradually until the end of the synchronization process.

At the initial stage of friction, the maximum temperature of the target gear ring friction cone appears at both ends of the contact surface. Then the maximum temperature of the friction cone appears only at the larger round end of surface

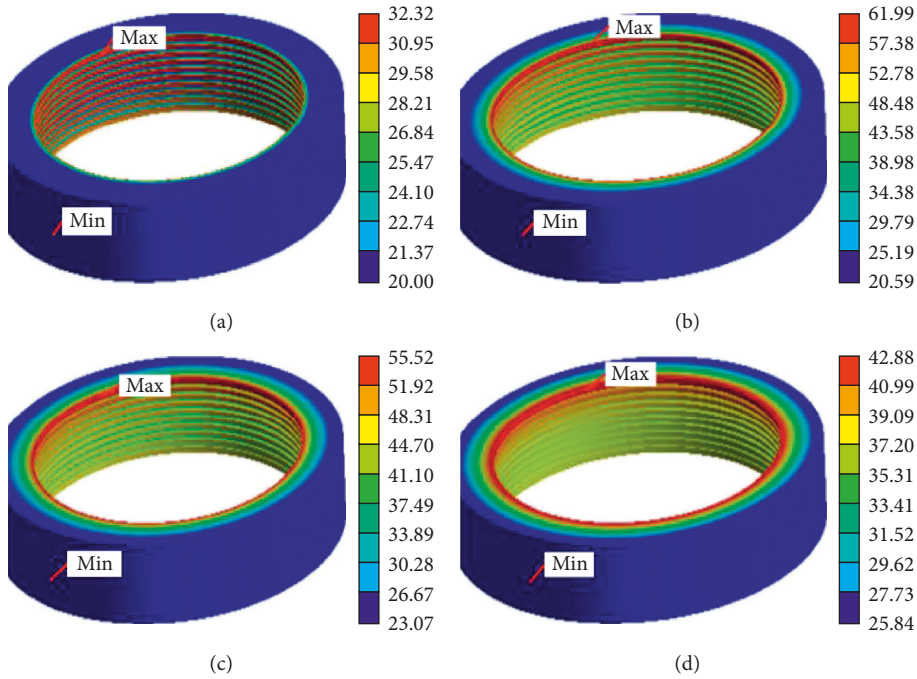

Figure 9: Surface temperature distribution of the synchronous ring. (a) $t = 0.035$ s, (b) $t = 0.678$ s, (c) $t = 1.143$ s, and (d) $t = 1.5$ s.

with the friction process. The temperature distribution of the friction cone tends to be uniform gradually. Note that the energy dissipation through heat conduction on the friction surface is the main determinant of the gear ring temperature rise, instead of convective heat transfer.

The maximum temperature of the synchronizer ring inner cone appears at all ring gears at the initial stage of friction. Then the maximum temperature of the synchronizer ring appears only at the smallest ring gear with the friction process. Therefore, the smaller the inner diameter of synchronizer ring gear is, the thicker the ring gear is. So that the energy dissipation of ring gear surface with smaller inner diameter is slower through heat conduction, and the temperature is higher than the ring gear surface with bigger inner diameter.

The temperature of friction surface under different working conditions is shown in Figure 10. The maximum temperature of friction surface increases about 1.8°C for every additional 50 N of the synchronous load. While the maximum temperature of friction surface increases about 1.1°C for every additional 200 r/min shift speed difference between the two ends of the synchronizer.

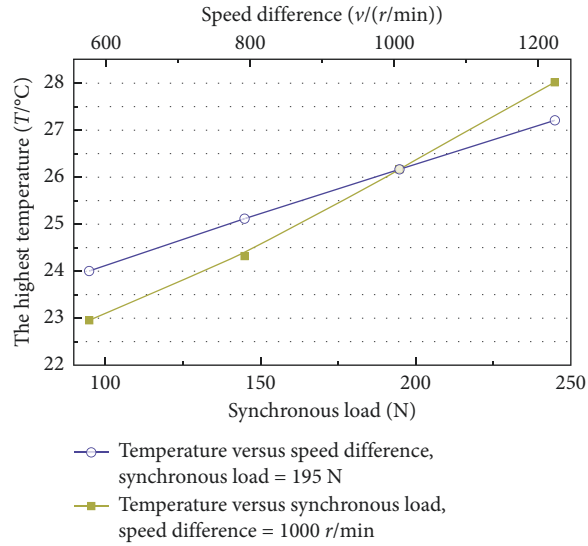

Figure 10: Variation law of temperature under different working conditions.

5.2. Friction Coefficient Analysis. The torque of the friction is obtained from torque-speed sensor under different working conditions, and the friction coefficient is calculated as follows:

$$\mu = \frac{T_S \sin \alpha}{F_S \cdot R}, \tag{13}$$

where T_S is the cone torque, F_S is the shifting force, α is the half-cone angle, and R is the cone radius. Hence, friction coefficient changing regularities of the friction cone under different working conditions are shown in Figure 11.

The friction coefficient changing regularities of the friction cone are the same under different conditions basically. The friction coefficient declines rapidly first and then tends to be stable slowly during the synchronization process. The experimental data about friction coefficient have fluctuations because of the coaxiality of test bench and surrounding electromagnetic interference. The analysis of friction coefficient changing regularity lays the foundation for establishing an effective friction coefficient compensation control strategy.

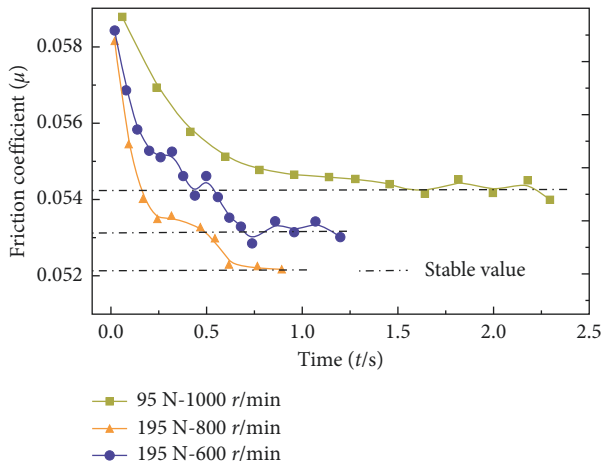

FIGURE 11: Variation law of friction coefficient of the friction cone under different working conditions.

6. Conclusions

In order to improve the shift quality further, the friction coefficient changing regularities of the friction cone and the temperature rise of friction surface during the synchronization process were investigated. The thermal-structural coupling model was established through tribo-thermodynamic analysis. The relevant experiment was carried out as well. Main results are summarized as follows:

(1) The error between the experimental and simulated results is controlled within 3%, which verifies the accuracy of the thermo-structural coupling model.

(2) The maximum temperature of synchronous ring friction surface increases 1.8°C for every additional 50 N of shift force, while increases 1.1°C for every additional 200 *r*/min shift speed difference.

(3) The friction coefficient declines rapidly firstly and then tends to be stable slowly during the synchronization process. The result of friction coefficient changing regularity lays a good theoretical basis for establishing an effective friction coefficient compensation control strategy.

Data Availability

The data used to support the findings of this study are available from the corresponding author upon request.

Conflicts of Interest

The authors declare that they have no conflicts of interest.

Acknowledgments

This work was supported by the National Natural Science Foundation of China (Grant no. 51505263); Six Talent Peaks Project in Jiangsu Province, China (Grant no. XNYQC-010); and the Natural Science Foundation of Shandong Province, China (Grant no. ZR2016EL15).

References

[1] D. T. Qin, M. Y. Yao, S. J. Chen, and S. K. Lyu, "Shifting process control for two-speed automated mechanical transmission of pure electric vehicles," *International Journal of Precision Engineering & Manufacturing*, vol. 17, no. 5, pp. 623–629, 2016.

[2] G. Wang and R. Fu, "Impact of brake pad structure on temperature and stress fields of brake disc," *Advances in Materials Science and Engineering*, vol. 2013, Article ID 872972, 9 pages, 2013.

[3] J. Bao, Z. Li, D. Hu, Y. Yin, and T. Liu, "Frictional performance and temperature rise of a mining nonasbestos brake material during emergency braking," *Advances in Materials Science and Engineering*, vol. 2015, Article ID 867549, 7 pages, 2015.

[4] C. Jo, J. Ko, H. Yeo, T. Yeo, S. Hwang, and H. Kim, "Cooperative regenerative braking control algorithm for an automatic-transmission-based hybrid electric vehicle during a downshift," *Proceedings of the Institution of Mechanical Engineers, Part D: Journal of Automobile Engineering*, vol. 226, no. 4, pp. 457–467, 2012.

[5] E.-H. Zhao, B. Ma, and H.-Y. Li, "Study on the high temperature friction and wear behaviors of Cu-based friction Pairs in wet clutches by pin-on-disc tests," *Advances in Materials Science and Engineering*, vol. 2017, Article ID 6373190, 8 pages, 2017.

[6] S. Beer and R. Ginosar, "A model for supply voltage and temperature variation effects on synchronizer performance," *IEEE Transactions on Very Large Scale Integration Systems*, vol. 23, no. 11, pp. 2461–2472, 2015.

[7] Z. G. Chen, Y. M. Shao, and T. C. Lim, "Non-linear dynamic simulation of gear response under the idling condition," *International Journal of Automotive Technology*, vol. 13, no. 4, pp. 541–552, 2012.

[8] I. Kovacevic, M. Djelosevic, G. Tepic, and S. Milisavljevic, "Influential parameters and numerical simulation of heat generated in the process of friction stir welding," *Materials Science*, vol. 22, no. 3, pp. 348–353, 2016.

[9] M. Li, M. M. Khonsari, D. M. C. McCarthy, and J. Lundin, "On the wear prediction of the paper-based friction material in a wet clutch," *Wear*, vol. 334-335, pp. 56–66, 2015.

[10] M. Li, M. M. Khonsari, N. Lingesten, P. Marklund, D. M. C. McCarthy, and J. Lundin, "Model validation and uncertainty analysis in the wear prediction of a wet clutch," *Wear*, vol. 364-365, pp. 112–121, 2016.

[11] P. Marklund, R. Mäki, R. Larsson, E. Höglund, M. M. Khonsari, and J. Jang, "Thermal influence on torque transfer of wet clutches in limited slip differential applications," *Tribology International*, vol. 40, no. 5, pp. 876–884, 2007.

[12] P. Marklund and R. Larssona, "Wet clutch friction characteristics obtained from simplified pin on disc test," *Tribology International*, vol. 41, no. 9-10, pp. 824–830, 2008.

[13] A. Bejan, "Theory of heat transfer-irreversible refrigeration plants," *International Journal of Heat & Mass Transfer*, vol. 32, no. 9, pp. 1631–1639, 1989.

[14] B. Li, W. Ge, H. Liu, and K. Wang, "Automatic manual transmission shift control strategy based on shift displacement following compensation," *Journal of the Balkan Tribological Association*, vol. 22, no. 2, pp. 1156–1166, 2016.

[15] Z. Zhang, X. Shi, and D. Guo, "Dynamic temperature rise mechanism and some controlling factors of wet clutch engagement," *Mathematical Problems in Engineering*, vol. 2016, Article ID 6530213, 12 pages, 2016.

[16] M. Mansouri, K. Holgerson, M. Khonsari, and W. Aung, "Thermal and dynamic characterization of wet clutch engagement with provision for drive torque," *Journal of Tribology*, vol. 123, no. 2, pp. 313–323, 2001.

[17] Q. Chen, H. Shu, L. Chen, W. Tu, and C. Liao, "Analysis on temperature field of electromagnetic clutch of in-wheel motor for micro-electric vehicle," *International Journal of Electric & Hybrid Vehicles*, vol. 8, no. 2, p. 109, 2016.

[18] A. Irimescu, S. S. Merola, C. Tornatore, and G. Valentino, "Development of a semi-empirical convective heat transfer correlation based on thermodynamic and optical measurements in a spark ignition engine," *Applied Energy*, no. 157, pp. 777–788, 2015.

[19] X. Ming, "3D models of thermo-mechanical coupling of grinding tooth and numerical analysis," *Chinese Journal of Mechanical Engineering*, vol. 44, no. 5, pp. 17–24, 2008.

[20] D. Zhu, X. Zhang, and H. Ding, "Tool wear characteristics in machining of nickel-based superalloys," *International Journal of Machine Tools and Manufacture*, vol. 64, no. 1, pp. 60–77, 2013.